Cerebral Cortex, February 2018;28: 713–725

doi: 10.1093/cercor/bhx002
Advance Access Publication Date: 6 July 2017
Original Article

ORIGINAL ARTICLE

Connectivity of the Cingulate Sulcus Visual Area (CSv) in the Human Cerebral Cortex

Andrew T. Smith[1], Anton L. Beer[2], Michele Furlan[1] and Rogier B. Mars[3,4]

[1]Department of Psychology, Royal Holloway, University of London, Egham TW20 0EX, UK, [2]Institut für Psychologie, Universität Regensburg, 93053 Regensburg, Germany, [3]Department of Experimental Psychology and Centre for Functional fMRI of the Brain (FMRIB), Nuffield Department of Clinical Neurosciences, University of Oxford, Oxford OX3 9DU, UK and [4]Donders Institute for Brain, Cognition and Behaviour, Radboud University, 6525 EN Nijmegen, The Netherlands

Address correspondence to Andrew T. Smith, Department of Psychology, Royal Holloway, University of London, Egham TW20 0EX, UK.
Email: a.t.smith@rhul.ac.uk

Abstract

The human cingulate sulcus visual area (CSv) responds selectively to visual and vestibular cues to self-motion. Although it is more selective for visual self-motion cues than any other brain region studied, it is not known whether CSv mediates perception of self-motion. An alternative hypothesis, based on its location, is that it provides sensory information to the motor system for use in guiding locomotion. To evaluate this hypothesis we studied the connectivity pattern of CSv, which is completely unknown, with a combination of diffusion MRI and resting-state functional MRI. Converging results from the 2 approaches suggest that visual drive is provided primarily by areas hV6, pVIP (putative intraparietal cortex) and PIC (posterior insular cortex). A strong connection with the medial portion of the somatosensory cortex, which represents the legs and feet, suggests that CSv may receive locomotion-relevant proprioceptive information as well as visual and vestibular signals. However, the dominant connections of CSv are with specific components of the motor system, in particular the cingulate motor areas and the supplementary motor area. We propose that CSv may provide a previously unknown link between perception and action that serves the online control of locomotion.

Key words: cingulate, CSv, self-motion, V6, VIP

Introduction

Interest in the neural substrates of visual motion perception has recently focused strongly on self-motion (egomotion). In primates, 2 cortical regions, the dorsal middle superior temporal area (MSTd) and the ventral intraparietal area (VIP), have long been known to contain neurons that are selectively sensitive to optic flow (Tanaka and Saito 1989; Duffy and Wurtz 1991) and to direction of heading (Duffy and Wurtz 1995; Bremmer et al. 2002). Electrical stimulation of these regions can influence heading judgments (Britten and van Wezel 2002; Zhang and Britten 2011) suggesting that they may contribute directly to perceptual awareness, although reversible inactivation impairs heading only in the case of MSTd (Chen et al. 2016) suggesting that VIP may not mediate perception. Many MSTd and VIP neurons also receive vestibular input (Duffy 1998; Gu et al. 2006; Chen et al. 2011b; Fetsch et al. 2012), consistent with a role in encoding self-motion. A third cortical region that is involved in visual heading has emerged more recently: area VPS (visual posterior sylvian), which also responds to both visual and vestibular stimuli (Chen et al. 2011a). As for MSTd, inactivation of this region impairs visual heading judgments (Chen et al. 2016).

In the human brain, putative homologs of macaque MST (Dukelow et al. 2001; Huk et al. 2002; Kolster et al. 2010) and VIP (Bremmer et al. 2001) have been identified. These have been

shown to be involved in encoding optic flow (Smith et al. 2006; Wall et al. 2008; Cardin et al. 2012). However, a new paradigm exposes a limitation in the ability of human MST (hMST) to signal self-motion. When an array of optic flow patches is presented, hMST responds almost as strongly as to a single patch (Wall and Smith 2008), even though the overall stimulus is inconsistent with self-motion. In putative VIP (pVIP), the response is only about half that to a single patch, implying some selectivity for self-motion. At least 2 other areas show greater selectivity than hMST (Cardin and Smith 2010). One is human V6 (hV6), a region identified in humans only quite recently (Pitzalis et al. 2006) and thought to be the homolog of macaque V6 (Galletti et al. 1991). The other is PIC (posterior insular cortex), which is located adjacent to vestibular area PIVC (parieto-insular vestibular cortex) and responds to both visual and vestibular stimulation (Frank et al. 2014).

The most surprising discovery arising from the multipatch paradigm is that the strongest specificity to visual self-motion yet demonstrated occurs in a region not previously studied in any detail, not previously associated with optic flow processing and not located within the dorsal processing stream. This is the cingulate sulcus visual area (CSv). Here, a strong response can be elicited by a single optic flow patch but the response is almost completely abolished when an array of optic flow patches is substituted (Wall and Smith 2008). Recent studies (Antal et al. 2008; Fischer et al. 2012) confirm the role of CSv in visual self-motion processing. An additional piece of evidence implicating CSv in self-motion processing is that it receives vestibular as well as visual input (Smith et al. 2012). A possible homolog of CSv has recently been reported in the macaque brain (Cottereau et al. 2017) but as yet it is not known whether this region is important for perceptual awareness of heading direction.

CSv is defined in terms of its responses to sensory stimuli. However its location, isolated from all other visual and vestibular areas but located close to motor areas, suggests that it may also be involved in motor control. It is possible that CSv serves to supply sensory information to the motor system. Key to evaluating this hypothesis and understanding the functions of CSv is to identify its connectivity with other brain regions. In this study, we use a combination of diffusion MRI and functional connectivity analysis in a first attempt to identify the cortical connections of CSv in healthy human volunteers. The 2 methodologies (functional connectivity and diffusion-based tractography) provide independent but complimentary estimates of connectivity in the in vivo brain (Damoiseaux and Greicius 2009). By applying both methods in the same set of brains, we overcome some of the limitations associated with each method (Jbabdi and Johansen-Berg 2011). Converging results may be regarded as providing a reliable estimate of the cortical connectivity of CSv.

Methods

A series of analyses investigating the functional and structural connectivity of CSv was performed. First, CSv was localized in individual subjects using previously established methods (Wall and Smith 2008). Since the cingulate cortex consists of a number of separate regions, each with a unique connectivity profile (Beckmann et al. 2009), we then used diffusion MRI to identify each of these cingulate regions in each participant and establish to which region CSv belongs. Third, we used the same diffusion data to investigate the whole-brain connectivity of CSv. Fourth, we used resting-state functional MRI (fMRI) to explore the whole-brain functional connectivity of CSv and compared the results to those obtained with diffusion MRI. Finally, we examined the structural and functional connectivity of CSv with specific target areas in the visual, parietal, and frontal cortex.

Data were collected from 12 healthy volunteers (7 females, median age 23.5 years) who participated in the experiment in accordance with approval from the Royal Holloway Research Ethics Committee. During scans, participants lay supine in a 3 T Siemens TIM Trio MRI scanner equipped with a 32-channel head coil. Each participant was scanned on 4 occasions. On one occasion, resting-state fMRI data and diffusion MRI data were acquired. In the other 3 sessions, functional data were acquired during various visual localizer tasks (details below). In one, CSv was localized. In another, retinotopic mapping was performed. In the third, hMT and hMST were localized and in addition a high-quality 3D T_1-weighted anatomical scan (MDEFT, Deichmann et al. 2004) was acquired (160 sagittal slices, 1 × 1 × 1 mm voxel size). This anatomical scan, which has high contrast between gray and white matter (WM), was used for normalization to standard space and for segmentation, cortical reconstruction and flattening. Faster 3D anatomical scans (MP-RAGE, Siemens) were acquired on the other 3 occasions to assist with co-registration across scans.

Localization of CSv and Other Visually Responsive Areas in Individual Participants

A previously established localizer was used to identify CSv, as well as hV6, pVIP, and PIC (Wall and Smith 2008; Cardin and Smith 2010). (Note that PIC was labeled as PIVC by Cardin and Smith 2010; PIC has been identified more recently and shown to be adjacent to PIVC; Frank et al. 2014). The localizer consisted of 2 time-varying optic flows (light dots on a dark background). The first was egomotion-compatible optic flow that cycled smoothly through spiral space to simulate back-and-forth spiral motion of the observer. The second was an egomotion-incompatible 3 × 3 array of similar spiral motions. Visual stimuli were projected onto a rear-projection screen positioned in the end of the scanner bore. Because a large visual field is beneficial for localizing these areas, the stimuli were viewed via a monocular magnifying optical device that gave a 60° diameter image. The device was positioned over the participant's preferred eye and the other eye was occluded. Each stimulus was presented for 3 s in an event-related design, with intertrial intervals (ITIs) in which the screen was blank apart from a central fixation spot. The ITIs varied between 2 and 10 s, following a Poisson probability distribution. Each scan run had 32 trials (16 per condition), presented in a pseudorandom order, and lasted approximately 5 min. Six such scan runs were conducted. Participants were continuously engaged in a color counting task at fixation. Contrasting the activity elicited by the 2 stimuli isolates regions (CSv, hV6, and pVIP) that favor egomotion-compatible flow from those that respond well to any flow stimuli. Data were acquired with the following parameters: 36 slices, voxel size = 3 × 3 × 3 mm, repetition time = 2500 ms, echo time = 31 ms. Parallel imaging (GRAPPA, factor 2) was used. The time series data were analyzed within the general linear model (GLM) using BrainVoyager QX 2.3 (BrainInnovation) according to our previously described methods. From the thresholded *t*-map, a region of interest (ROI) was defined for each of the 3 visual areas in each hemisphere.

hMT and hMST were defined based on a standard method (Dukelow et al. 2001; Huk et al. 2002). A circular patch of dots (8° diameter) was presented with its center placed 10° to the left or right of fixation. The stimuli were viewed binocularly via a mirror. Blocks of 15 s in which the dots were static were alternated with blocks of 15 s in which the dots moved alternately inward and

outward along the radial axes, creating alternating contraction and expansion. Sixteen blocks (8 static and 8 moving) were presented in each scan run; one run was completed with the stimulus on the left and another with it on the right. With this procedure, hMT and hMST can be differentiated in terms of the absence or presence, respectively, of ipsilateral activity when the moving and static stimuli are contrasted. Again, ROIs were defined based on a thresholded *t*-map derived within a GLM analysis in accordance with our previously described methods. Although hMST is likely comprised of 2 or more motion-responsive sub-regions with large receptive fields (Amano et al. 2009; Kolster et al. 2010), these were not separated as doing so would have exceeded the spatial resolution of our connectivity analyses.

Visual areas V1, V2, V3, and V3A were identified with a standard retinotopic mapping procedure employing an 8 Hz counterphasing checkerboard wedge stimulus (a 24° sector) of radius 12° viewed binocularly via a mirror. Check size was scaled by eccentricity in approximate accordance with the cortical magnification factor. The wedge rotated clockwise at a rate of 64 s/cycle and 8 cycles were presented. This stimulus was presented twice to each participant, and the data from the 2 scan runs were averaged to give the final retinotopic maps. Conventional phase maps were created on a flattened representation of the gray matter. The boundaries of the visual areas were defined manually based on standard criteria.

Diffusion MRI

Diffusion-weighted images were acquired in each participant by a spin-echo sequence with echoplanar readout (65 axial slices, 2 × 2 × 2 mm voxel size at a 192 × 192 mm field of view, 9300 ms repetition time, 94 ms echo time, 90° flip angle). Diffusion weighting was isotropically distributed along 64 directions (Jones et al. 2002) using a *b*-value of 1000 s × mm^{-2}. Three sets of diffusion-weighted data were acquired for all but one participant. For technical reasons, only 2 sets were acquired in one participant. This participant's results were not anomalous. In addition, 6 volumes with no diffusion weighting (*b*-zero) were acquired, in pairs interleaved with the 3 sets of diffusion-weighted scans.

Data were processed using the diffusion tools from the FMRIB Software Library (FSL) (Smith et al. 2004). Images were corrected for eddy currents and head motion using affine registration to the mean *b*-zero reference volume. Diffusion vectors were corrected for estimated head motion parameters. Data from the 3 acquisitions were combined to improve the signal-to-noise ratio. Voxel-wise probability distributions of a maximum of 2 (constrained by automatic relevance detection) anisotropic diffusion compartments were then calculated using Markov Chain Monte Carlo sampling (Behrens et al. 2007).

Tractography-Based Parcellation

We first tested whether CSv shows a connectivity profile that is distinct from other cingulate regions. A connectivity-based parcellation of the cingulate cortex of each participant was performed following Beckmann et al. (2009). A ROI including the territory ventral and anterior to the genu of the corpus callosum, the anterior cingulate, mid-cingulate, and cingulate motor areas, and the posterior cingulate was created in Montreal Neurological Institute (MNI) space. This ROI was subsequently warped to each participant's structural space and used as a seed region for parcellation tractography. Probabilistic tractography was run from each voxel of the ROI to each voxel in the rest of the brain (downsampled to 5 mm isotropic resolution to reduce the computational load) in diffusion space using the following parameters: 5000 samples from each ROI voxel, maximum of 2000 steps, step length of 0.5 mm, and a curvature threshold of 0.2. A connectivity matrix between the ROI voxels and each other brain voxel was derived and used to generate a symmetric cross-correlation matrix in which each element indicates the correlation between 2 ROI voxels' connectivity profiles. The rows in this cross-correlation matrix were permuted using *k*-means clustering to define 9 clusters of voxels sharing similar connectivity profiles.

Whole-Brain Connectivity of CSv Based on Diffusion MRI

In order to investigate the WM connections of CSv with other cortical regions, a surface-based analysis of track terminations was adopted (Beer et al. 2011). For this analysis, cortical reconstructions were created from each hemisphere by Freesurfer version 5 (Martinos Center for Biomedical Imaging). Probabilistic tracking based on the diffusion data was seeded at CSv vertices of the WM surface of each hemisphere. Left and right CSv served as separate seeds. Tracking parameters were as in the parcellation analysis except that 20 000 samples were tracked per seed vertex. The resulting track frequency (f_{track}) maps were log-scaled in order to account for size differences in seed regions. Log-scaled track frequencies were divided by the maximum in each brain resulting in track probabilities [$P_{track} = \log(f_{track})/\max(\log(f_{track}))$]. Subsequently, track probabilities of voxels at the white/gray matter boundary (1 mm into WM) of each hemisphere were projected and spherically registered to the cortical surface of an average brain. Then, track probabilities were averaged across the hemispheres of all brains and thresholded. A supplementary whole-brain analysis was conducted on the number of subjects with supra-threshold track probabilities ($P_{thres} = 0.5$) at a given location (Beer et al. 2011). This analysis indicates the reproducibility of the tractography solution across subjects.

Connectivity of CSv with Specific Target Masks Based on Diffusion MRI

Group-averaged whole-brain probabilistic fiber tracking profiles tend to neglect less pronounced tracks or tracks to brain regions with substantial variability across brains. To exploit the increased precision offered by the use of functionally defined ROIs, WM connectivity was also estimated in each hemisphere between CSv and a number of specific motion-sensitive brain areas in the occipital and parietal cortex. These were V3A, hV6, pVIP, PIC, hMT, and hMST, localized as described above. With probabilistic fiber tracking, even non-existent WM connections have a low but non-zero track probability. In order to test our tracking results against chance, the track probability expected under the null hypothesis was estimated based on a reference region. Early visual areas (V1, V2, and V3) were chosen as the reference, on the assumption that these areas are probably not directly connected to CSv. However, as V1 and perhaps also V2/V3 are likely connected indirectly with any area that is visually responsive, they provide a more conservative reference (high baseline) than would non-visual areas. Left and right CSv were each analyzed for connectivity in left and right hemispheres so that both ipsilateral and contralateral connections could be identified.

Whole-Brain Resting-State Functional Connectivity of CSv

Resting-state fMRI data were acquired in each participant in the same session as the diffusion-weighted images. For each

participant, 144 volumes of whole-brain blood oxygen level-dependent (BOLD) fMRI data were collected using the following parameters: 36 axial slices, voxel size = 3 × 3 × 3 mm, repetition time = 2500 ms, echo time = 31 ms, GRAPPA factor 2. Participants were instructed to lie still with their eyes open and not fall asleep during the scan. For each participant and each hemisphere, we created a separate resting-state functional connectivity analysis looking at the connectivity of CSv with the whole brain while taking confounding factors of WM, cerebrospinal fluid (CSF), and head movement into account.

The following preprocessing steps were applied: Discarding the first 6 volumes, motion correction, nonbrain removal, spatial smoothing using a Gaussian kernel of FWHM 5 mm, grand-mean intensity normalization of the entire 4D data set by a single multiplicative factor, high-pass temporal filtering (Gaussian-weighted least-squares straight line fitting with sigma = 50.0 s). Functional data were then aligned to structural space using linear registration and the structural scan was transformed to standard MNI152 space using nonlinear registration. The functional data were submitted to a probabilistic independent component analysis (Beckmann and Smith 2004). The first 10 identified components were inspected and components consisting of obvious artifacts (movement, activity in veins or ventricles) were removed from the data. The resulting data were used for further analyses.

For each participant, the location of CSv as determined by the localizer task was transformed to resting-state functional space and the first major Eigen time series representing activity in that area of interest was calculated separately for the left and the right hemisphere CSv. We also calculated the major Eigen time series in masks representing the WM and CSF across the whole-brain volumes; these were derived using FSL's tissue segmentation tool FAST (Zhang et al. 2001). Time series representing head motion were extracted using MCFLIRT (Jenkinson and Smith 2001). These 8 confound time series (WM, CSF, and 6 time series representing head movements) were included as confound regressors in every resting-state analysis. To assess results at the group level, subject-level images of parameter estimates were submitted to a mixed-effects analysis using automatic outlier detection (Woolrich et al. 2004; Woolrich 2008). As for diffusion-based tractography, left and right CSv were each analyzed for connectivity in both ipsilateral and contralateral hemispheres.

Resting-State Functional Connectivity with Specific Target Masks

We established the resting-state functional connectivity between CSv and the same specific visual target areas that were examined with diffusion MRI. This was done by calculating the average parameter estimate of CSv functional connectivity across the voxels within the visual target region.

Finally, functional connectivity with a further set of target areas based on previously published probabilistic atlases (www.rbmars.dds.nl/CBPatlases.htm) was also established. ROIs in the parietal cortex were based on the results of a previous parcellation of the lateral parietal cortex (Mars et al. 2011), which identified 10 areas and created probabilistic masks of these in standard space. Each mask was thresholded at 50% of the population, meaning that we investigated functional connectivity of CSv with voxels that belonged to a particular parietal cortex area in >50% of the population. Since the original parietal parcellation was only performed on the right hemisphere, the ROIs were mirrored along the mid-sagittal plane to create masks in the left hemisphere. ROIs in the medial frontal cortex and ventrolateral frontal cortex were created in the same manner, using the results of previous frontal cortical parcellation studies focusing on these areas (Sallet et al. 2013; Neubert et al. 2014).

Results

Localization of CSv

CSv was localized in each individual participant with previously published procedures (Wall and Smith 2008). In order to ensure that our localization of CSv is compatible with this and subsequent reports, we transformed all participants' binarized CSv activation hotspots to standard space and overlaid them. This showed CSv to be localized in the posterior part of the mid-cingulate sulcus (Fig. 1*a*). The group aggregate clusters had centers of gravity of [9 −24 44] and [−10 −26 41] in the 2 hemispheres (Fig. 1*a*), which is consistent with previous reports (Wall and Smith 2008; Cardin and Smith 2010).

Cingulate Parcellation and CSv

In order to test whether CSv shows a connectivity profile that is distinct from other cingulate areas, we performed a connectivity-based parcellation (Beckmann et al. 2009). In this technique, voxels are grouped together based on their shared connectivity with the entire brain, identifying separate cortical units with distinctive connectivity (Johansen-Berg et al. 2004).

Based on the maps published in Beckmann et al. (2009), we hypothesized that CSv is part of their caudal cingulate zone (CCZ). In order to test this hypothesis, we submitted their original cingulate ROI to parcellation based on our participants' diffusion MRI data. Similar to Beckmann and colleagues, we identified a cluster at the posterior end of the mid-cingulate cortex, just anterior to the dorsal extension of the cingulate sulcus (Fig. 1*b*). The center of gravity of this cluster in the 2 hemispheres was [9 −24 43] and [−9 −26 43], which is consistent with it being CCZ as identified by Beckmann et al. Consistent with our hypothesis, CSv overlaps with this cluster in both hemispheres, with a focus in the fundus of the cingulate sulcus. This

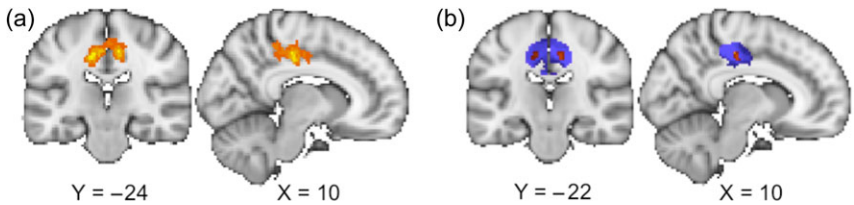

Figure 1. CSv localization. (*a*) Location of CSv (red/yellow) in MNI standard space as determined by functional imaging using a visual localizer. Yellow represents the strongest activation, in the depths of the cingulate sulcus. (*b*) Location of CCZ (blue/purple) as determined by a connectivity-based (diffusion MRI) parcellation, in the same standard space. Color represents number of participants (purple highest). Both results are based on group data (12 participants) and are thresholded to show only voxels belonging to CSv/CCZ in at least 4 participants.

finding suggests that CSv, which appears as an island of visual activity in fMRI studies with visual localizers, is a discrete area with connectivity that is different from all other nearby regions.

Whole-Brain Connectivity of CSv Based on Diffusion MRI

We next created a group whole-brain map to identify the most prominent connections of CSv based on the same diffusion MRI data. Figure 2*a*,*b* shows a map of the cortical track terminations for tracks seeded in CSv. A conservative threshold (P_{thres} = 0.5) as described in the literature (Behrens et al. 2003) was chosen in order to reduce the likelihood of false positives. Tracks seeded in ipsilateral CSv (Fig. 2*a*) primarily terminated along the caudal anterior cingulate sulcus and gyrus. Dorsal and posterior track terminations were observed in the paracentral gyrus/sulcus and dorsal parts of the subparietal sulcus and precuneus (extending to the dorsal parieto-occipital sulcus). Furthermore, CSv tracks were observed in 2 distinct regions of the corpus callosum (posterior midbody and rostral body) and the thalamus. Track probabilities at the lateral surface of the brain were low; significant track terminations were limited to the anterior insula and the superior frontal gyrus. Track terminations of the contralateral CSv (Fig. 2*b*) were much less pronounced and were primarily observed in the paracentral gyrus and sulcus (partially overlapping with the contralateral CSv). The results of the whole-brain track termination maps were very similar for left and right CSv, suggesting structural symmetry. As a check on the generalizability of the results across participants, a whole-brain map showing the number of brains in which track probability exceeded threshold was also generated (see Supplementary Fig. S1). The overall pattern of results was very similar to that in Figure 2, suggesting that the results are not due to a small number of outlier participants.

Connectivity of CSv with Specific Visual Target Regions Based on Diffusion MRI

The group whole-brain maps in Figure 2 showed little evidence of connectivity between CSv and occipital cortex and provided few hints concerning the source of the visual inputs to CSv. Note, however, that a conservative threshold was applied in that analysis. To provide greater sensitivity, we tested the connectivity strength between CSv and a number of specific target areas that have previously been shown to be relevant to visually driven perception of egomotion. Four higher-order visual areas were identified in individual participants using previously established methods and the average probability of CSv tracks was determined for each of these regions. This was done separately for each hemisphere. The locations of the visual target regions are shown in Figure 2*c* along with the seed region, CSv. They agree well with our previous work (Furlan et al. 2014).

The probability of connectivity with CSv is shown for each visual region in Figure 3. The results were very similar for the 2 hemispheres and are, therefore, combined to show ipsilateral (R-R and L-L) and contralateral (R-L and L-R) connections. Track probability with V1, V2, and V3 was similar for all 3 areas and was lower than any other area examined. This suggests that it is unlikely that CSv receives strong direct input from any of these areas. In view of the similarity, the 3 areas were pooled and were used as a reference for statistical comparisons. We reasoned that ROI-to-ROI track probabilities that significantly exceeded the track probabilities between CSv and this reference region were likely not due to chance. Note that if our assumption of no

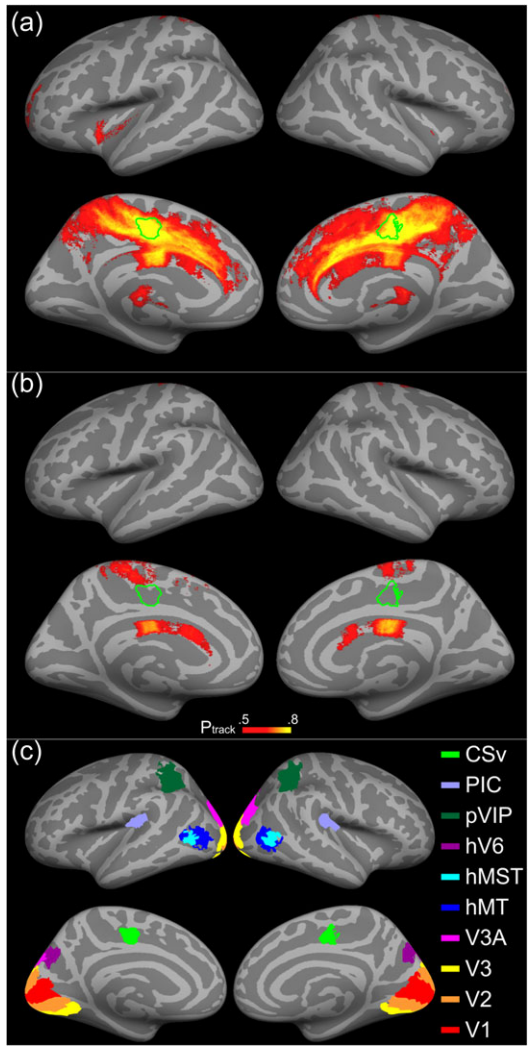

Figure 2. Whole-brain CSv connectivity from diffusion MRI. The images show the mean track probabilities (P_{track}) of the whole group (n = 12) projected onto the inflated cortical surfaces of the average brain and thresholded to P_{thres} = 0.5. (*a*) Ipsilateral connectivity (tracks of left CSv within left hemisphere and right CSv within right hemisphere), (*b*) contralateral connectivity (e.g., right CSv with left hemisphere). (*c*) Seed (CSv) and target cortical visual areas regions identified with visual localizers, defined separately in each individual but illustrated as voxels overlapping in at least 4 participants. CSv is also transposed to panels (a) and (b) as a green outline.

connections between CSv and early visual areas (V1–V3) is false, then the chance level would be even lower than that estimated by this reference region. We, therefore, compared (by paired t-test, n = 12) the track probability seen in each other area studied with this reference. In addition, we counted for each area the number of brains (out of 12) with a track probability greater than the reference. For ipsilateral connectivity, the number was 10 for pVIP and 11 for V3A, hV6, and PIC. For contralateral connectivity, it was 10 for pVIP, V3A, and PIC and 12 for hV6.

Because of their strong motion sensitivity, potential sources of visual information in CSv might be hMT and/or hMST. Both areas were successfully localized in every participant. The center of gravity of the combined MT/MST region was [47 −71 3] in the right and [−47 −75 5] in the left hemisphere. However, as can be seen in Figure 3, track probability was not significantly greater in either hMT or hMST than in V1–V3. This suggests that direct projections to CSv from hMT/hMST are weak or absent.

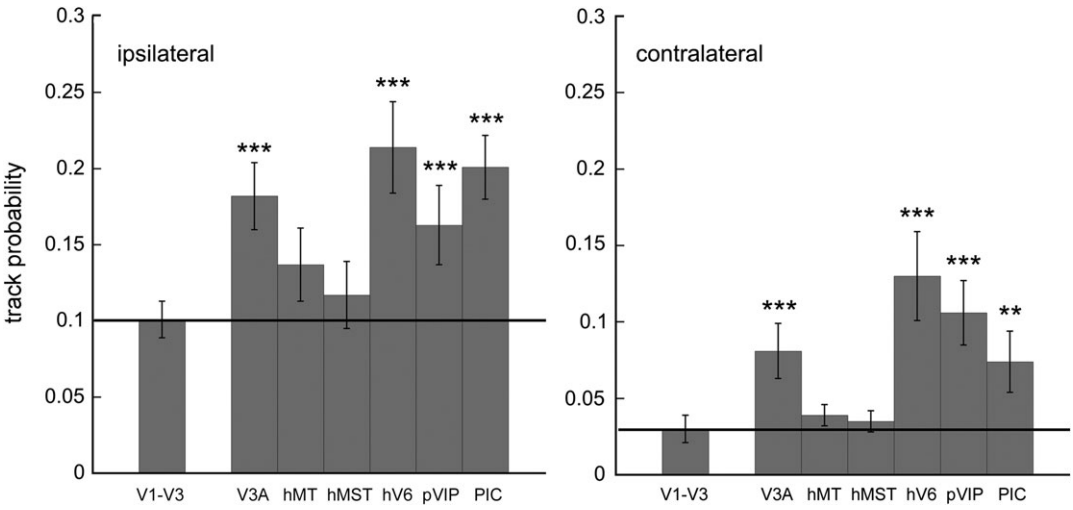

Figure 3. CSv connectivity with target visual areas from diffusion MRI. The results of probabilistic tractography with CSv as the origin (seed) are shown for each of a number of cortical visual areas, localized in individual participants. Left and right CSv were analyzed separately and track probability, averaged across participants ($n = 12$), is shown separately for ipsilateral (left panel) and contralateral (right panel) connections. The average result obtained for V1–V3 (horizontal line) is used as a baseline for statistical comparison by t-test. Key to statistical significance: ***$P < 0.001$; **$P < 0.01$.

Given their specificity to egomotion-compatible retinal motion, we hypothesized that hV6, pVIP, and PIC may be sources of visual input to CSv and would, therefore, show strong connectivity with CSv. These regions were localized in each participant using the same visual stimulus that was employed to localize CSv. On average, the location of hV6 was [20 –79 33] in the right and [–15 –83 31] in the left hemisphere. Area pVIP is more difficult to localize using the egomotion localizer because the 9-patch stimulus elicits a robust response and localization, therefore, relies on a more modest differential response. Nevertheless, the average center of gravity of pVIP, [30 –48 55] in the right and [–30 –49 58] in the left hemisphere, was in line with previous reports. However, the overlap between participants was much lower than for hV6 or hMST. The mean location of area PIC was [38 –38 18] in the right hemisphere and [–41 –40 17] in the left. As can be seen in Figure 3, significant hV6 connectivity was evident with both ipsilateral and contralateral CSv, consistent with our hypothesis. Track probability was higher for ipsilateral than contralateral V6, as might be expected. Area pVIP also showed significant connectivity with both ipsilateral and contralateral CSv. The high degree of variability across brains in the location of pVIP might explain why these tracks were not evident in the whole-brain maps (Fig. 2). PIC showed strong connectivity with ipsilateral CSv. The contralateral connection probability was somewhat lower than for hV6 or pVIP but still significantly higher than that of V1–V3.

A surprising result from the tractography ROI analysis was that V3A appeared to be significantly connected with CSv. Human V3A is strongly associated with motion processing. However (unlike hV6 and pVIP), it is not sensitive to the difference between egomotion-compatible and egomotion-incompatible flow (Wall and Smith 2008).

Whole-Brain Resting-State Functional Connectivity of CSv

We next aimed to determine the resting-state functional connectivity of CSv with the whole brain. Resting-state fMRI provides a measure of the spontaneous covariance between brain regions. The networks of covariance described during rest are often similar to those co-activating during task performance (Smith et al. 2009). Although resting-state functional connectivity is an indirect measure that does not exclusively reflect structural connections, it has been shown to depend on structural connections (O'Reilly et al. 2013) and to be capable of identifying known anatomical connections (Mars et al. 2011). Following previous studies using resting-state fMRI data (Mars et al. 2013), we here focus on the positive correlations, since the relationship between negative fMRI correlations and structural connections is uncertain.

The dominant time course of each individual's CSv cluster was extracted (separately for left and right CSv) from the preprocessed resting-state data and used in a first-level regression analysis to determine the extent to which it explained the time course of each voxel in the brain, while accounting for variance explained by the time courses of the cerebrospinal fluid and WM. The resulting first-level statistical images where then submitted to a group-level analysis. The result is shown in Figure 4. The functional connectivity of right and left CSv was largely similar. The results, therefore, confirm that CSv has a symmetrical organization, as suggested by the diffusion data. On the medial surface of the brain, the ipsilateral functional connectivity showed strong similarity to the counterpart results from diffusion MRI (Fig. 2). There was significant functional connectivity along the cingulate sulcus and posterior-to-middle cingulate gyrus and the paracentral lobule. Importantly, the medial maps showed connectivity in a small dorsal portion of the parieto-occipital sulcus, likely corresponding to hV6. The map differed from the diffusion result in that the medial connections were almost as strong in the contralateral as the ipsilateral hemisphere.

Also in contrast to the diffusion MRI map, strong CSv connectivity was apparent on the lateral surface of the brain: around the precentral gyrus, along the postcentral gyrus extending into the posterior parietal cortex and the supramarginal gyrus. A large cluster of functional connectivity was found in the insula, which merged with the inferior part of the precentral cluster; this was apparent but much less prominent in the diffusion data.

Resting-State Functional Connectivity with Specific Visual Target Regions

We next established the resting-state functional connectivity between CSv and the specific visual target areas we examined with diffusion MRI. As in the case of diffusion MRI, the results were (with one exception, see below) similar for the right and left hemispheres and were combined to yield a single ipsilateral and a single contralateral connection strength for each visual area. These are shown in Figure 5. In general, the results showed good agreement with the diffusion data of Figure 3. Areas V1–V3 showed no evidence of functional connectivity with CSv. In contrast, significant CSv connectivity with hV6 was evident, both ipsilaterally and contralaterally. The same applied to pVIP although connectivity was only just significant in the contralateral case. pVIP was the single exception to the statement that right and left hemispheres gave similar results. Right pVIP showed significant connectivity with both right CSv and left CSv but in left pVIP we could not detect connectivity with either left or right CSv (not illustrated). This might reflect functional laterality. Note, however, that there was no sign of a similar hemispheric asymmetry in structural connectivity based on diffusion MRI. The strongest resting-state connectivity of any area was with ipsilateral PIC. Contralateral PIC also showed numerically strong mean connectivity, albeit with an unusually high variance across participants.

An important difference between the results of the 2 methods concerns V3A. This region showed pronounced connectivity with CSv in the diffusion data (Fig. 3) but this was absent in the resting-state data (Fig. 5). Another difference was that area hMST, which showed no CSv connectivity in the diffusion data, showed functional connectivity, although only ipsilaterally. At present, it is unclear whether these findings reflect differences between structural and functional connectivity or methodological limitations.

In summary, the functional connectivity analysis confirmed that CSv is connected with hV6, pVIP, and PIC, but failed to confirm connectivity with V3A and instead suggests possible connectivity with ipsilateral hMST.

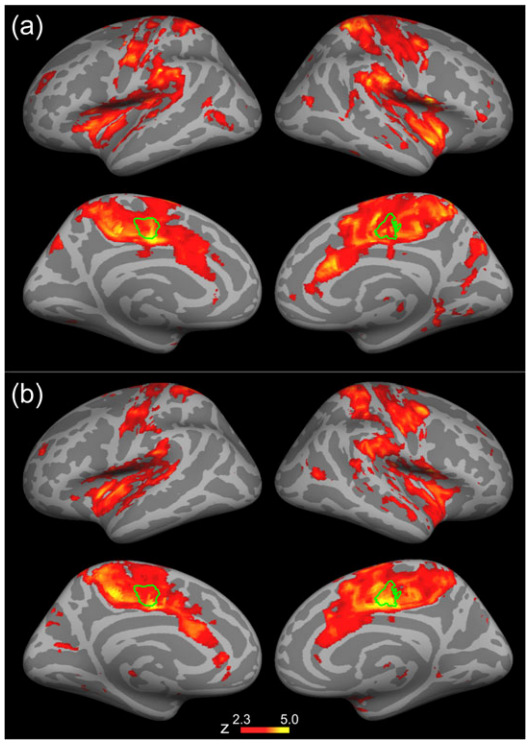

Figure 4. Whole-brain CSv resting-state functional connectivity. Images are whole-brain *z*-statistical images from a group analysis ($n = 12$) for the CSv ROI, projected onto the inflated cortical surface of the average brain and thresholded at $z > 2.3$. (*a*) Ipsilateral connectivity, (*b*) contralateral connectivity, as in Figure 2.

Resting-State Functional Connectivity With Parietal and Frontal Cortex

The whole-brain analysis in Figure 4 shows functional connectivity with lateral parts of the brain including parts of both parietal and frontal cortex. This was not evident in the diffusion MRI data but it is of interest because CSv coincides with the CCZ cluster of Beckmann et al. (2009) who reported a high

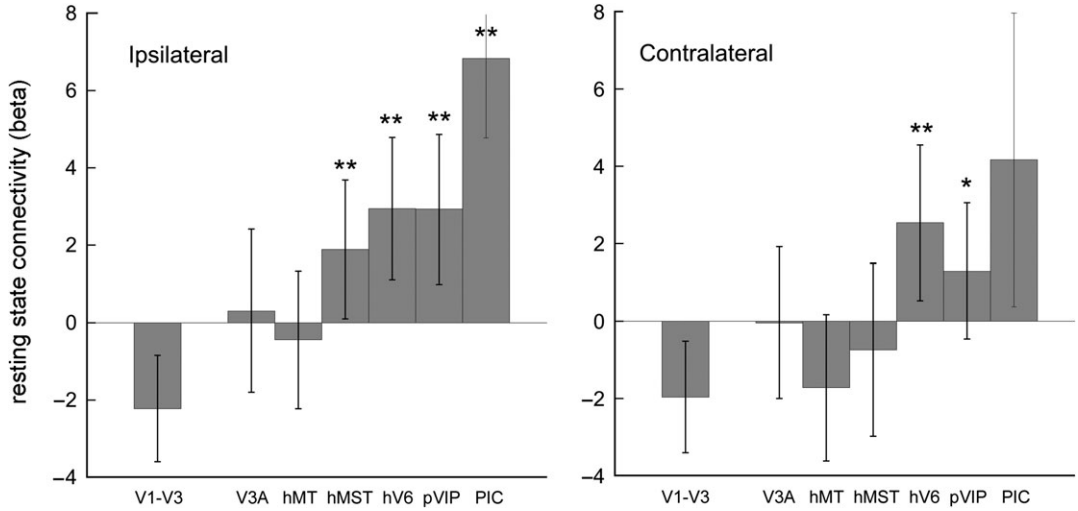

Figure 5. CSv functional connectivity with individually localized visually responsive cortical areas. The results of an analysis of resting-state functional connectivity with CSv are shown for each of a number of cortical visual areas, localized in individual participants. Left and right CSv were analyzed separately and connectivity, averaged across participants ($n = 12$), is shown separately for ipsilateral and contralateral connections. For comparability with Figure 3, the results for V1–V3 are used for statistical comparison by *t*-test. Key to statistical significance: $^{**}P < 0.01$; $^{*}P < 0.05$.

connection probability between CCZ and parietal cortex based on diffusion MRI. We, therefore, examined the functional connectivity of CSv with a number of ROIs in parietal and frontal cortex. Only ipsilateral connections were examined.

The parietal ROIs were based on the probabilistic atlas of Mars et al (2011). In the superior parietal lobule (SPL), we tested the functional connectivity of CSv with a lateral anterior region including the banks of the intraparietal sulcus, a medial anterior region overlapping with area 5, a lateral posterior region that has been proposed to overlap MIP and perhaps posterior AIP, and a medial posterior region that shows overlap with area 7A as defined by Scheperjans et al. (2008). We obtained CSv functional connectivity only with the most anterior parts of the SPL (Fig. 6*a*). Interestingly, the anterior lateral ROI overlapped with area VIP as defined previously by Bremmer et al. (2001). This provides a further indication of functional connectivity between CSv and pVIP.

In the inferior parietal lobule (IPL), we investigated CSv functional connectivity with 5 ROIs, namely the most anterior part of the inferior parietal cortex overlapping with the parietal operculum, the anterior and posterior supramarginal gyrus, and the anterior and posterior angular gyrus (Fig. 6*b*). CSv functional connectivity was confined to the 2 anterior-most locations examined. These regions correspond well with the expected location of PIC.

The whole-brain analysis in Figure 4 also shows functional connectivity with parts of lateral frontal cortex. We again used previously published anatomical maps to specify more fully where it is found. We first investigated the interactions of CSv with areas of the medial frontal cortex outside the narrow cingulate cortex ROI of Beckmann et al. (2009). Specifically, we investigated the functional connectivity of CSv with the supplementary motor area (SMA), the pre-SMA, and medial areas 9 and 10 as mapped by Sallet et al. (2013). The results are shown in Figure 7*a*. As has already been noted based on the group map of Figure 4, SMA showed strong connectivity with CSv. However, the other medial regions, including pre-SMA, which is directly adjacent to SMA, showed no functional connectivity with CSv.

The inferior frontal cortex contains a gradient of areas ranging from agranular premotor cortex via dysgranular areas to fully granular prefrontal areas. These areas were recently mapped by Neubert et al. (2014) and we used their probabilistic atlas to investigate the functional connectivity between CSv and premotor areas 6v and 6r and the more anteriorly located areas 44d, 44v, 45A, and 47. Similar to its functional connectivity with the SMAs, CSv showed a strong coupling with the ventral premotor cortex, in particular with area 6r (Fig. 7*b*). Anteriorly, CSv functional connectivity was far less prominent, although some interaction with area 44v was apparent.

Discussion

We have made a detailed study of the connectivity of CSv using 2 independent approaches: tractography based on diffusion-weighted MRI and functional connectivity based on correlations in the resting-state BOLD response. The same brains were studied in both cases and the results compared. Both approaches are somewhat error-prone but in quite different ways, so our strategy was to look for commonalities in the results and to draw firm conclusions only when we found them. Our principle aim was to establish connectivity with sensory cortex and in particular to establish the likely sources of the visual information known to be present in CSv. However, our results also show a pattern of connectivity that

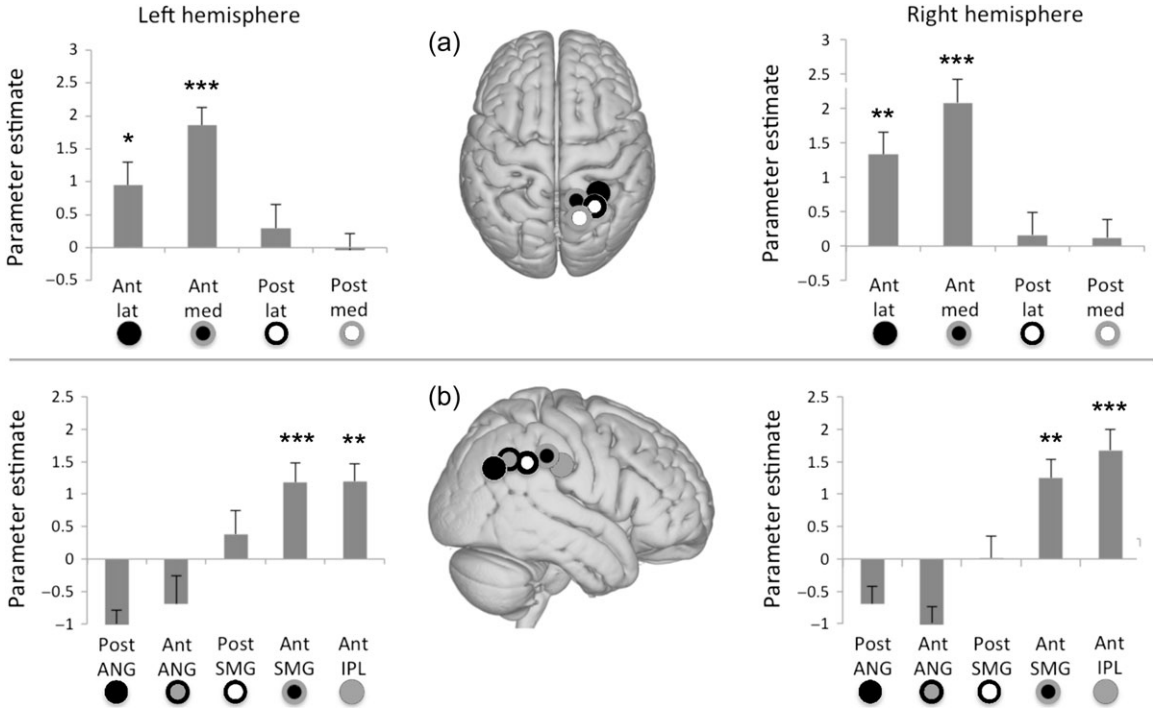

Figure 6. CSv functional connectivity with areas in parietal cortex. Middle panels show the approximate location of the centers of gravity of the parietal cortex ROIs from Mars et al. (2011) (illustrated for only one hemisphere). Bar graphs show the corresponding ipsilateral group CSv functional connectivity parameter estimates and standard errors for each hemisphere. (*a*) Anterior lateral SPL, anterior medial SPL, posterior lateral SPL, and posterior medial SPL. (*b*) Anterior IPL, anterior SMG, posterior SMG, anterior ANG, and posterior ANG. Key to statistical significance: ***$P < 0.001$; **$P < 0.01$; *$P < 0.05$.

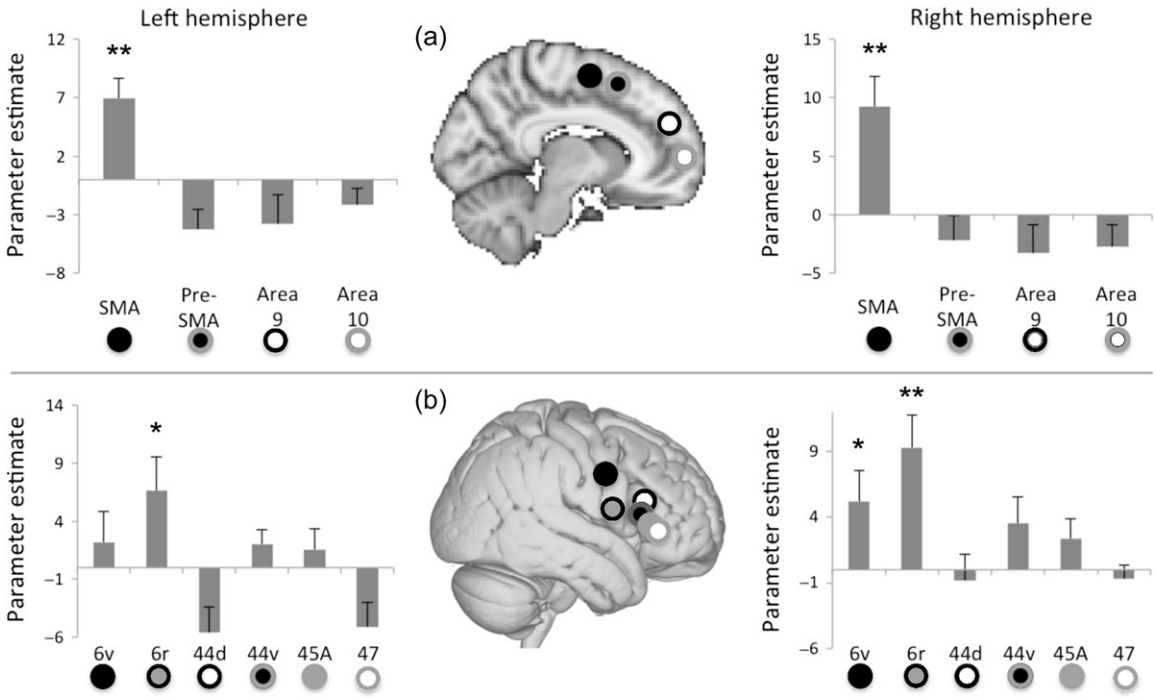

Figure 7. CSv functional connectivity with areas in frontal cortex. Middle panels show the approximate location of the centers of gravity of frontal cortex ROIs from Sallet et al. (2013) and Neubert et al. (2014). Bar graphs show the corresponding ipsilateral group CSv functional connectivity parameter estimates and standard errors. (*a*) Medial areas SMA, pre-SMA, Area 9 and Area 10. (*b*) Ventrolateral areas 6v, 6r, 44d, 44v, 45A and 47. Key to statistical significance: $^{**}P < 0.01$; $^{*}P < 0.05$.

suggests strong involvement in motor functions. We will consider these 2 aspects separately.

Sensory Input to CSv

CSv responds to optic flow that simulates self-motion and to vestibular stimulation. It is, therefore, perhaps surprising that neither visual nor vestibular cortical regions were prominent in the group whole-brain connectivity maps of CSv (Figs 2 and 4). However, a more sensitive analysis based on independently defined visual ROIs provided evidence concerning the likely source of visual drive. The earliest visual areas (V1–V3) did not show functional connectivity with CSv and gave the lowest track probabilities with diffusion MRI. It is, therefore, likely that direct visual input to CSv arises elsewhere, although early visual cortex is likely to be indirectly connected. We found clear evidence for a connection with area hV6, in the parieto-occipital sulcus. This was evident in the ROI analyses from both methods (Figs 3 and 5) and it was discernable in the resting-state group analysis (Fig. 4). Consistent with this, a recent study of the connections of functionally defined hV6 (Tosoni et al. 2014) has shown signs of functional connectivity in a small region of the posterior cingulate that might correspond to CSv. In contrast, primate tracer studies (Colby et al. 1988; Galletti et al. 2001) involving injections in V6 did not yield labeled cells in the cingulate cortex. V6 is thought to be concerned with self-motion in both humans (Pitzalis et al. 2006; Cardin and Smith 2010) and monkeys (Galletti et al. 1999). It responds primarily to moving stimuli and responds more strongly to coherent optic flow than to random motion (Pitzalis et al. 2010) or even to egomotion-incompatible coherent motion (Cardin and Smith 2010), providing strong evidence that it is concerned with visual cues to self-motion. We cannot determine the direction of information flow from our data but it is likely that the ascending pathway is from hV6 to CSv because hV6 shows the pattern typical of early visual areas in which each hemisphere responds mainly to contralateral stimuli (Pitzalis et al. 2006), whereas CSv responds to both contralateral and ipsilateral stimuli (Fischer et al. 2012). Consistent with this, connectivity between CSv and hV6 is bilateral and symmetrical in our data, that is left and right V6 each connect with both left and right CSv. Additional evidence for this direction of excitatory information flow is that selectivity for egomotion-compatible motion is more developed in CSv than in hV6 (Cardin and Smith 2010).

Good converging evidence from the 2 methods for connectivity with CSv was also evident in the case of pVIP. Like hV6, this region is associated with visual cues to self-motion (Bremmer et al. 2001; Kovacs et al. 2008) and it is, therefore, a candidate for providing visual drive to CSv. The evidence for connectivity was a little weaker in our data for pVIP than for hV6 but it is possible that this merely reflects the greater uncertainty and variability in the definition of pVIP noted earlier. pVIP may also be an important source of vestibular drive to CSv. Our whole-brain maps do not suggest strong connections between CSv and PIVC, the most prominent cortical vestibular region. Human pVIP responds to vestibular stimuli, although only weakly (Smith et al. 2012). It is unlikely that hV6 provides vestibular signals to CSv because it appears not to have vestibular sensitivity.

Our results also show clear evidence for connectivity between PIC and CSv. In the functional connectivity data, ipsilateral PIC shows the strongest connectivity of any region (Fig. 5). In the diffusion data, the evidence is equally compelling, although in this case PIC does not stand out, hV6 and pVIP having comparable track probabilities. Connectivity with contralateral PIC is also suggested by the results of both methods. Area PIC has been shown to be responsive to both visual

and vestibular stimuli (Frank et al. 2014) and visual responses are greater for egomotion-compatible optic flow than for an array of flow patches (Cardin and Smith 2010). A possible homolog of PIC in the nonhuman primate could be VPS (Chen et al. 2016). Tracer studies in the squirrel monkey show that this region (previously known as T3) densely projects to the posterior cingulate sulcus region (Guldin et al. 1992). These factors make it a very plausible candidate for supplying visual and/or vestibular information to CSv, although we cannot be sure of the direction of information flow between the 2 areas.

Two other visual areas emerge as possible sources of visual drive to CSv but with lower certainty because the connection was apparent with only one of the 2 methods we used. The first is V3A, which showed very convincing signs of bilateral connectivity in the diffusion data but not in the resting-state data. One possible explanation for this inconsistency could be that V3A is connected with CSv but this connection is inactive in the resting state. However, methodological limitations cannot be ruled out, including a lack of statistical power for revealing the connectivity. The second is hMST, which showed significant connectivity with CSv in the functional data, although only in the ipsilateral hemisphere, but showed only weak, nonsignificant signs of connectivity with CSv in the diffusion data. The ipsilateral functional (but not structural) connectivity between hMST and CSv could reflect poly-synaptic (rather than monosynaptic) connections. V3A and hMST both respond well to coherent motion but show much less selectivity for self-motion than pVIP, hV6, or PIC, making them possible although less likely direct sources for CSv. Further study, therefore, seems warranted.

Motor Connections of CSv

A striking feature of our group connectivity maps is strong connectivity with a large portion of the cingulate region, including the entire posterior cingulate and the caudal portion of the anterior cingulate. Ipsilateral connectivity in this region was evident in the data from both techniques. The functional connectivity map suggests equally strong contralateral connectivity. The diffusion data suggest that contralateral connections are present but considerably weaker, though this might simply reflect limitations in tracking fibers through the corpus callosum.

In macaques, the cingulate sulcus contains several distinct motor regions that together occupy both banks of the sulcus over much of its length (Picard and Strick 1996). The separate functions of these areas remain to be elaborated, but the more caudal regions are somatotopically organized and stimulation can elicit limb movements (Luppino et al. 1991). A plausible interpretation is that these regions may be concerned specifically with locomotor functions. In humans, motor tasks involving the hand and foot, but not tasks involving the mouth or tongue, elicit BOLD responses in the cingulate (Amiez and Petrides 2014), consistent with a similar organization to macaques. These responses extend over a large portion of the cingulate, again broadly encompassing the posterior and caudal anterior zones. Our data, therefore, suggest that CSv is strongly connected with cingulate motor regions. Accordingly, an important function of CSv may be to feed visual and possibly vestibular information about self-motion into a medial motor system concerned with control of locomotion.

Connectivity is also evident, again from both techniques, in the ascending portion of the cingulate sulcus (also known as the marginal sulcus). This sulcus forms the boundary between the precuneus and the paracentral lobule and connectivity appears to extend anteriorly into the paracentral lobule. The paracentral lobule contains the primary somatosensory representation of the leg and foot (Kapreli et al. 2007; Zlatkina et al. 2016). This raises the possibility that CSv receives not only visual and vestibular signals but also somatosensory afferents, all of which feed into motor control. Visual and vestibular signals do not appear to be integrated in CSv, given its insensitivity to the relationship (congruent or incongruent) between signals in the 2 modalities (Billington and Smith 2015), so CSv may simply collate information from different senses for motor use as required.

The group connectivity maps showed that CSv connectivity extends further anteriorly along the medial surface, as far as the SMA. In the case of functional connectivity (Fig. 4), there were signs that connectivity exists in 2 distinct dorso-medial regions, somatosensory cortex and SMA, and not in the intervening medial primary motor cortex (although there was evidence of connectivity in parts of the lateral motor cortex, absent in the diffusion data). Connectivity with SMA (but not pre-SMA) was also evident in the quantitative analysis of Figure 7. The functions of the SMA are subject to debate (see Nachev et al. 2008 for review) but it is located adjacent to the leg and foot representations in motor cortex and stimulation can result in complex movements involving multiple body parts, in both macaque (Graziano and Aflalo 2007) and human (Fried et al. 1991), suggesting that SMA may be concerned with locomotion. On the lateral surface, the functional (but not diffusion) connectivity data also showed CSv connectivity with area 6r in ventral premotor cortex (Fig. 7).

The motor system occupies an extensive set of cortical regions that appear to have related and overlapping functions. Our data suggest a specific pattern of connectivity between CSv and some of these regions (particularly the cingulate motor regions and SMA), but not others. This pattern appears consistent with a role in guiding locomotion. Our interpretation is speculative and will require confirmation. Evidence on the direction of flow of information between CSv and the motor system is lacking, as is a fully developed theory of any such motor role of CSv.

Interpretational Limitations

Our hypothesis that CSv may link perception and action is based on nondirectional brain imaging connectivity metrics and further research will be required for confirmation. Connectivity measures based on brain imaging have certain limitations. For example, diffusion-based tractography provides only an indirect measure of structural connectivity, identifying the path of lowest diffusion hindrance rather than tracing the axons themselves. Some recent studies have questioned the use of diffusion MRI tractography to establish the long-range connections of cortical areas (Reveley et al. 2015). Moreover, a difficult trade-off between sensitivity and selectivity exists (Thomas et al. 2014). The gold standard of connectivity research remains the use of invasive tracers in model species, such as the macaque monkey (see Morecraft et al. 2009 for an overview), even though some recent studies show that tractography and tracer data show converging results if certain methodological considerations are taken into account (Donahue et al. 2016; Mars et al. 2016). However, it is important to point out that diffusion MRI tractography and resting-state functional connectivity do not necessarily aim to obtain the same results as

invasive tracer studies. Rather than aiming to identify the monosynaptic connections between specific cortical regions, the strength of MRI-based methods lies in elucidating the place of a region within the larger whole-brain network. Our study produced information of this kind in relation to CSv, by applying a number of different but complementary approaches. First, we employed tractography in order to parcellate the cingulate cortex. This analysis showed that CSv overlaps with human CCZ. Second, we used tractography in conjunction with resting-state functional connectivity, 2 methods that have very different strengths and weaknesses, placing most emphasis on results that showed a convergence between the 2 approaches. Our results suggest that CSv is located at the interface of the brain's perceptual and motor systems. The strength of whole-brain, in-vivo neuroimaging methods is that they can elucidate such patterns, even if one would contest the specificity of the method in describing any one particular connection and its directionality.

Supplementary Material

Supplementary material is available at *Cerebral Cortex* online.

Funding

The Medical Research Council UK and the Dutch Organization for Scientific Research (452-13-015 to R.B.M.).

Notes

We are grateful to V. Azorina for assistance with data analysis and M. W. Greenlee for helpful discussions. *Conflict of Interest*: None declared.

References

Amano K, Wandell BA, Dumoulin SO. 2009. Visual field maps, population receptive field sizes, and visual field coverage in the human MT+ complex. J Neurophysiol. 102:2704–2718.

Amiez C, Petrides M. 2014. Neuroimaging evidence of the Anatomo-Functional Organization of the human cingulate motor areas. Cereb Cortex. 24:563–578.

Antal A, Baudewig J, Paulus W, Dechent P. 2008. The posterior cingulate cortex and planum temporale/parietal operculum are activated by coherent visual motion. Vis Neurosci. 25: 17–26.

Beckmann C, Smith S. 2004. Probabilistic independent component analysis for functional magnetic resonance imaging. IEEE Trans Med Imaging. 23:137–152.

Beckmann M, JohansenBerg H, Rushworth MF. 2009. Connectivity-based parcellation of human cingulate cortex and its relation to functional specialization. J Neurosci. 29: 1175–1190.

Beer AL, Plank T, Greenlee MW. 2011. Diffusion tensor imaging shows white matter tracts between human auditory and visual cortex. Exp Brain Res. 213:299–308.

Behrens T, Johansen-Berg H, Jbabdi S, Rushworth M, Woolrich M. 2007. Probabilistic diffusion tractography with multiple fibre orientations: what can we gain? NeuroImage. 34:144–155.

Behrens TEJ, Johansen-Berg H, Woolrich MW, Smith SM, Wheeler-Kingshott CAM, Boulby PA, Barker GJ, Sillery EL, Sheehan K, Ciccarelli O, et al. 2003. Non-invasive mapping of connections between human thalamus and cortex using diffusion imaging. Nat Neurosci. 6:750–757.

Billington J, Smith AT. 2015. Neural mechanisms for discounting head-roll-induced retinal motion. J Neurosci. 35: 4851–4856.

Bremmer F, Duhamel JR, Hamed SB, Graf W. 2002. Heading encoding in the macaque ventral intraparietal area (VIP). Eur J Neurosci. 16:1554–1568.

Bremmer F, Schlack A, Shah N, Zafiris O, Kubischik M, Hoffmann K-P, Zillies K, Fink G. 2001. Polymodal motion processing in posterior parietal and premotor cortex: a human fMRI study strongly implies equivalencies between humans and monkeys. Neuron. 29:287–296.

Britten KH, van Wezel RJ. 2002. Area MST and heading perception in macaque monkeys. Cereb Cortex. 12:692–701.

Cardin V, Hemsworth L, Smith AT. 2012. Adaptation to heading direction dissociates the roles of human MST and V6 in the processing of optic flow. J Neurophysiol. 108:794–801.

Cardin V, Smith AT. 2010. Sensitivity of human visual and vestibular cortical regions to egomotion-compatible visual stimulation. Cereb Cortex. 20:1964–1973.

Chen A, DeAngelis GC, Angelaki DE. 2011a. Convergence of vestibular and visual self-motion signals in an area of the posterior sylvian fissure. J Neurosci. 31:11617–11627.

Chen A, DeAngelis GC, Angelaki DE. 2011b. Representation of vestibular and visual cues to self-motion in ventral intraparietal cortex. J Neurosci. 31:12036–12052.

Chen A, Gu Y, Liu S, DeAngelis GC, Angelaki DE. 2016. Evidence for a causal contribution of macaque vestibular, but not intraparietal, cortex to heading perception. J Neurosci. 36: 3789–3798.

Colby C, Gattas R, Olson R, Gross C. 1988. Topographical organization of cortical afferents to extrastriate visual area PO in the macaque: a dual tracer study. J Comp Neurol. 269: 392–413.

Cottereau BR, Smith AT, Rima S, Fize D, Héjja-Brichard S, Renaud L, Lejards C, Vayssière N, Trotter Y, Durand J-B. 2017. Processing of egomotion-consistent optic flow in the rhesus macaque cortex. Cereb Cortex. (in press).

Damoiseaux J, Greicius M. 2009. Greater than the sum of its parts: a review of studies combining structural connectivity and resting-state functional connectivity. Brain Struct Funct. 213:525–533.

Deichmann R, Schwarzbauer C, Turner R. 2004. Optimisation of the 3D MDEFT sequence for anatomical brain imaging: technical implications at 1.5 and 3 T. Neuroimage. 21: 757–767.

Donahue C, Sotiropoulos S, Jbabdi S, Hernandez-Fernandez M, Behrens T, Dyrby T, Coalson T, Kennedy H, Knoblauch K, Van Essen D, et al. 2016. Using diffusion tractography to predict cortical connection strength and distance: a quantitative comparison with tracers in the monkey. J Neurosci. 36:6758–6770.

Duffy CJ. 1998. MST neurons respond to optic flow and translational movement. J Neurophysiol. 80:1816–1827.

Duffy CJ, Wurtz RH. 1991. Sensitivity of MST neurons to optic flow stimuli. I. A continuum of response selectivity to large-field stimuli. J Neurophysiol. 65:1329–1345.

Duffy CJ, Wurtz RH. 1995. Responses of monkey MST neurons to optic flow stimuli with shifted centers of motion. J Neurosci. 15:5192–5208.

Dukelow SP, DeSouza JFX, Culham JC, van den Berg AV, Menon RS, Vilis T. 2001. Distinguishing subregions of the human MT+ complex using visual fields and pursuit eye movements. J Neurophysiol. 86:1991–2000.

Fetsch CR, Pouget A, DeAngelis GC, Angelaki DE. 2012. Neural correlates of reliability-based cue weighting during multisensory integration. Nat Neurosci. 15:146–154.

Fischer E, Bülthoff HH, Logothetis NK, Bartels A. 2012. Visual motion responses in the posterior cingulate sulcus: a comparison to V5/MT and MST. Cereb Cortex. 22: 865–876.

Frank SM, Baumann O, Mattingley JB, Greenlee MW. 2014. Vestibular and visual responses in human posterior insular cortex. J Neurophysiol. 112:2481–2491.

Fried I, Katz A, McCarthy G, Sass K, Williamson P, Spencer S, Spencer D. 1991. Functional organization of human supplementary motor cortex studied by electrical stimulation. J Neurosci. 11:3656–3666.

Furlan M, Wann JP, Smith AT. 2014. A representation of changing heading direction in human cortical areas pVIP and CSv. Cereb Cortex. 24:2848–2858.

Galletti C, Battaglini PP, Fattori P. 1991. Functional properties of neurons in the anterior bank of the parieto-occipital sulcus of the macaque monkey. Eur J Neurosci. 3:452–461.

Galletti C, Fattori P, Gamberini M, Kutz DF. 1999. The cortical visual area V6: brain location and visual topography. Eur J Neurosci. 11:3922–3936.

Galletti C, Gamberini M, Kutz DF, Fattori P, Luppino G, Matelli M. 2001. The cortical connections of area V6: an occipito-parietal network processing visual information. Eur J Neurosci. 13:1572–1588.

Graziano MSA, Aflalo TN. 2007. Mapping behavioral repertoire onto the cortex. Neuron. 56:239–251.

Gu Y, Watkins PV, Angelaki DE, DeAngelis GC. 2006. Visual and nonvisual contributions to 3-dimensional heading selectivity in the medial superior temporal area. J Neurosci. 26:73–85.

Guldin WO, Akbarian S, Grüsser OJ. 1992. Cortico-cortical connections and cytoarchitectonics of the primate vestibular cortex: a study in squirrel monkeys (*Saimiri sciureus*). J Comp Neurol. 326:375–401.

Huk AC, Dougherty RF, Heeger DJ. 2002. Retinotopy and functional subdivision of human areas MT and MST. J Neurosci. 22:7195–7205.

Jbabdi S, Johansen-Berg H. 2011. Tractography: where do we go from here? Brain Connect. 1:169–183.

Jenkinson M, Smith S. 2001. A global optimisation method for robust affine registration of brain images. Med Image Anal. 5:143–156.

Johansen-Berg H, Behrens TEJ, Robson MD, Drobnjak I, Rushworth MFS, Brady JM, Smith SM, Higham DJ, Matthews PM. 2004. Changes in connectivity profiles define functionally distinct regions in human medial frontal cortex. Proc Natl Acad Sci USA. 101:13335–13340.

Jones D, Williams S, Gasston D, Horsfield M, Simmons A, Howard R. 2002. Isotropic resolution diffusion tensor imaging with whole brain acquisition in a clinically acceptable time. Hum Brain Mapp. 15:216–230.

Kapreli E, Athanasopoulos S, Papathanasiou M, Van Hecke P, Kelekis D, Peeters R, Strimpakos N, Sunaert S. 2007. Lower limb sensorimotor network: issues of somatotopy and overlap. Cortex. 43:219–232.

Kolster H, Peeters R, Orban GA. 2010. The retinotopic organization of the human middle temporal area MT/V5 and its cortical neighbors. J Neurosci. 30:9801–9820.

Kovacs G, Raabe M, Greenlee MW. 2008. Neural correlates of visually induced self-motion illusion in depth. Cereb Cortex. 18:1779–1787.

Luppino G, Matelli M, Camarda R, Gallese V, Rizzolatti G. 1991. Multiple representations of body movements in medial area 6 and the adjacent cingulate cortex: an intracortical microstimulation study in the macaque monkey. J Comp Neurol. 311:463–482.

Mars R, Foxley S, Verhagen L, Jbabdi S, Sallet J, Noonan M, Neubert F, Andersson J, Croxson P, Dunbar R, et al. 2016. The extreme capsule fiber complex in humans and macaque monkeys: a comparative diffusion MRI tractography study. Brain Struct Funct. 221:4059–4071.

Mars RB, Jbabdi S, Sallet J, O'Reilly JX, Croxson PL, Olivier E, Noonan MP, Bergmann C, Mitchell AS, Baxter MG, et al. 2011. Diffusion-weighted imaging tractography-based parcellation of the human parietal cortex and comparison with human and macaque resting-state functional connectivity. J Neurosci. 31:4087–4100.

Mars RB, Sallet J, Neubert FX, Rushworth MF. 2013. Connectivity profiles reveal the relationship between brain areas for social cognition in human and monkey temporoparietal cortex. Proc Natl Acad Sci USA. 110:10806–10811.

Morecraft RJ, Ugolini G, Lanciego JL, Wouterlood FG, Pandya DN. 2009. Classic and contemporary neural tract tracing techniques. In: Johansen-Berg H, Behrens T, editors. Diffusion MRI: from quantitative measurement to in vivo neuroanatomy. Amsterdam: Elsevier. p. 273–308.

Nachev P, Kennard C, Husain M. 2008. Functional role of the supplementary and pre-supplementary motor areas. Nat Rev Neurosci. 9:856–869.

Neubert F, Mars R, Thomas A, Sallet J, Rushworth M. 2014. Comparison of human ventral frontal cortex areas for cognitive control and language with areas in monkey frontal cortex. Neuron. 81:700–713.

O'Reilly J, Croxson P, Jbabdi S, Sallet J, Noonan M, Mars R, Browning P, Wilson C, Mitchell A, Miller K, et al. 2013. A causal effect of disconnection lesions on interhemispheric functional connectivity in rhesus monkeys. Proc Natl Acad Sci USA. 110:13982–13987.

Picard N, Strick PL. 1996. Motor areas of the medial wall: a review of their location and functional activation. Cereb Cortex. 6:342–353.

Pitzalis S, Galletti C, Huang R-S, Patria F, Committeri G, Galati G, Fattori P, Sereno MI. 2006. Wide-field retinotopy defines human cortical visual area V6. J Neurosci. 26:7962–7963.

Pitzalis S, Sereno MI, Committeri G, Fattori P, Galati G, Patria F, Galletti C. 2010. Human V6: the medial motion area. Cereb Cortex. 20:411–424.

Reveley C, Seth AK, Pierpaoli C, Silva AC, Yu D, Saunders RC, Leopold DA, Ye FQ. 2015. Superficial white matter fiber systems impede detection of long-range cortical connections in diffusion MR tractography. Proc Natl Acad Sci USA. 112:E2820–E2828.

Sallet J, Mars R, Noonan M, Neubert F, Jbabdi S, O'Reilly J, Filippini N, Thomas A, Rushworth M. 2013. The organization of dorsal prefrontal cortex in humans and macaques. J Neurosci. 33:12255–12274.

Scheperjans F, Eickhoff S, Homke L, Mohlberg H, Hermann K, Amunts K, Zilles K. 2008. Probabilistic maps, morphometry, and variability of cytoarchitectonic areas in the human superior parietal cortex. Cereb Cortex. 18:2141–2157.

Smith AT, Wall MB, Thilo KV. 2012. Vestibular inputs to human motion-sensitive visual cortex. Cereb Cortex. 22:1068–1077.

Smith AT, Wall MB, Williams AL, Singh KD. 2006. Sensitivity to optic flow in human cortical areas MT and MST. Eur J Neurosci. 23:561–569.

Smith S, Fox P, Miller K, Glahn D, Fox P, Mackay C, Filippini N, Watkins K, Toro R, Laird A, et al. 2009. Correspondence of the brain's functional architecture during activation and rest. Proc Natl Acad Sci USA. 106:13040–13045.

Smith S, Jenkinson M, Woolrich M, Beckmann C, Behrens T, Johansen-Berg H, Bannister P, De Luca M, Drobnjak I, Flitney D, et al. 2004. Advances in functional and structural MR image analysis and implementation as FSL. Neuroimage. 23 (Suppl 1): S208–S219.

Tanaka K, Saito H. 1989. Analysis of motion of the visual field by direction, expansion/contraction, and rotation cells clustered in the dorsal part of the medial superior temporal area of the macaque monkey. J Neurophysiol. 62: 626–641.

Thomas C, Ye F, Irfanoglu M, Modi P, Saleem K, Leopold D, Pierpaoli C. 2014. Anatomical accuracy of brain connections derived from diffusion MRI tractography is inherently limited. Proc Natl Acad Sci USA. 111:16574–16579.

Tosoni A, Pitzalis S, Committeri G, Fattori P, Galletti C, Galati G. 2014. Resting-state connectivity and functional specialization in human medial parieto-occipital cortex. Brain Struct Funct. DOI10.1007/s00429-00014-00858-x.

Wall MB, Lingnau A, Ashida H, Smith AT. 2008. Selective visual responses to expansion and rotation in the human MT complex revealed by functional magnetic resonance imaging adaptation. Eur J Neurosci. 27:2747–2757.

Wall MB, Smith AT. 2008. The representation of egomotion in the human brain. Curr Biol. 18:191–194.

Woolrich M. 2008. Robust group analysis using outlier inference. NeuroImage. 41:286–301.

Woolrich M, Behrens T, Beckmann C, Jenkinson M, Smith S. 2004. Multilevel linear modelling for FMRI group analysis using Bayesian inference. NeuroImage. 21:1732–1747.

Zhang T, Britten KH. 2011. Parietal area VIP causally influences heading perception during pursuit eye movements. J Neurosci. 31:2569–2575.

Zhang Y, Brady M, Smith S. 2001. Segmentation of brain MR images through a hidden Markov random field model and the expectation maximization algorithm. IEEE Trans Med Imaging. 20:45–57.

Zlatkina V, Amiez C, Petrides M. 2016. The postcentral sulcal complex and the transverse postcentral sulcus and their relation to sensorimotor functional organization. Eur J Neurosci. 43:1268–1283.